Conference Proceedings

ASES National Solar Conference 2018

Boulder, Colorado August 5-8, 2018

ASES National Solar Conference 2018

A Low-Cost IoT Approach to Real-Time Cloud Motion Detection

Ian Smithpeter

Colorado State University, Fort Collins, CO (USA)

iansmithpeter@yahoo.com

Abstract

As solar energy accounts for a larger portion of power grids around the world, it becomes necessary to mitigate the power output variability caused by intermittent cloud cover. When applied to a photovoltaic (PV) array, this variability limits the percentage of energy in a power grid generated by solar power. This limitation applies to both grid tied and islanded power systems. Many strategies exist to mitigate these effects, including the use of backup generators but efficient hybrid solar power systems require accurate short-term forecasting of sharp changes to ground horizontal irradiance (GHI) to minimize fuel usage. This work describes an Internet of Things (IoT) network of inexpensive nodes equipped with pyranometers and explores a simplex optimization method of calculating cloud motion vectors (CMVs). The IoT network was successful in reliably measuring GHI but limited by the chosen communication modules. The simplex optimization method was found to be comparably accurate and marginally more stable in calculating CMVs when compared to the more commonly utilized Most Correlated Pair method.

Keywords: *Internet of Things, solar power, irradiance forecasting, distributed sensor network*

1. Introduction

Solar power output is directly related to either the observed ground horizontal irradiance (GHI) or direct normal irradiance (DNI). Solar power is often implemented in a hybrid system with a diesel generator to smooth power output across variable irradiance. Solar power output on days with full sun is easily modeled using a tool such as the PVLIB toolbox from Sandia National Laboratories (Stein et al., 2016) to predict maximum irradiance and subsequent solar power output from a system at any given time. Overcast days yield a fraction of the solar power output of clear days, but changes to instantaneous power output occur gradually and are easily mitigated. Days with intermittent cloud cover pose a challenge as the average power output can vary by 40% across a 15 minute window (Suri et al., 2014) and instantaneous power output can change by 80% within a 60 second window. To efficiently implement a solar-diesel power system without large, expensive energy storage it is necessary to accurately forecast short-term observed irradiance fluctuations caused by passing cloud shadows.

doi:10.18086/solar.2018.01.12 Available at http://proceedings.ises.org

One form of forecasting observed irradiance involves calculating cloud motion vectors (CMVs) to predict when a cloud shadow will cross an observation point. The first methods for calculating CMVs were derived in the 1960s using satellite imagery for weather forecasting purposes (Menzel, 2001). Since then, work has been done to calculate CMVs with the application to irradiance forecasting using sky-facing cameras (Chow et al., 2011, 2015; Urquhart et al., 2015) and arrays of pyranometers (Aryaputera et al., 2015; Bosch et al., 2013; Yang et al., 2014). This project explores a low-cost Internet of Things (IoT) solution for solar irradiance forecasting using a wireless network of pyranometers. It also provides a method for detecting intermittent cloud cover that causes sharp power variability and presents an alternate numerical method for calculating CMVs.

2. Network Setup

2.1 Overview of Test Location

The sensor network utilized for this study was installed at the Methane Emission Technology Evaluation Center (METEC) located at the Foothills Campus of Colorado State University. Adjacent to the Rocky Mountains in northern Colorado, this area is prone to rapid changes in cloud cover and is therefore a great location to observe irradiance variability. Twelve nodes with uncalibrated pyranometers were placed along the METEC perimeter, one reference node with a calibrated pyranometer was placed near the center of the site, and a gateway node that connected perimeter nodes to the internet was placed in a building on the east side. All node locations can be seen in Figure 1. The nodes span 250 meters East-West and 150 meters North-South giving a maximum inter-node spacing of 270 meters.

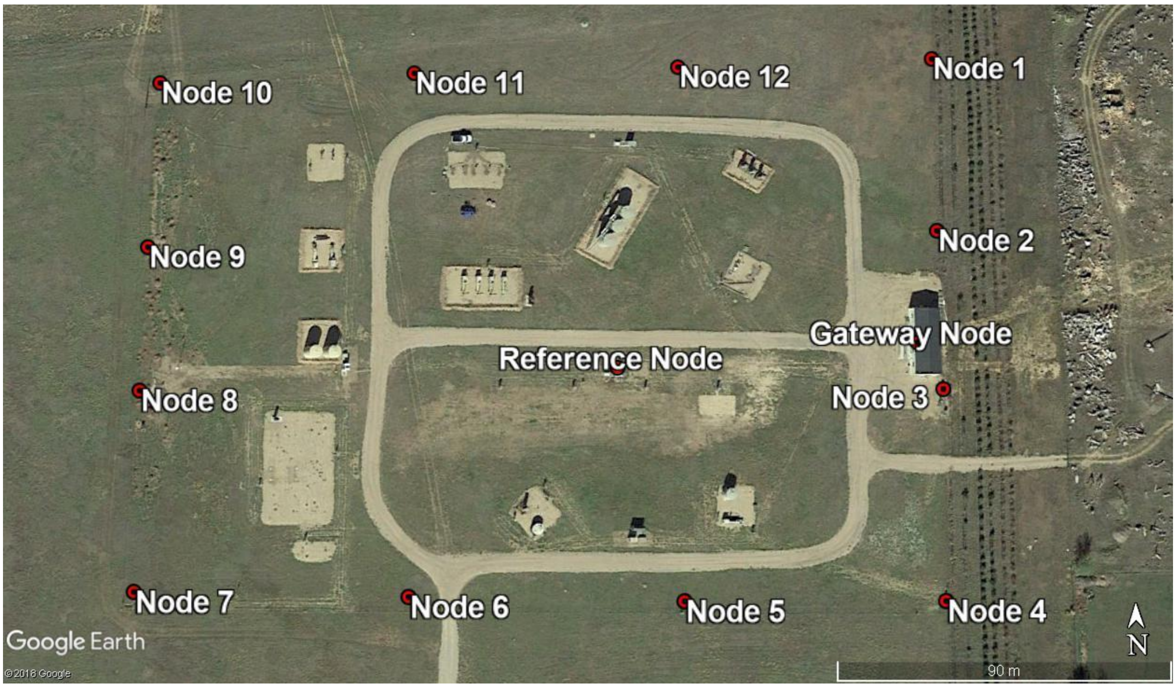

Figure 1: Sensor Node Locations

2.2 Hardware

Each of the perimeter nodes utilizes a STM Nucleo as the central processor. Voltage output from an uncalibrated photodetector pyranometer is measured using a 16-bit Analog-to-Digital Converter (ADC) while time and location information is provided by a GPS receiver. Readings are transmitted to the gateway node using an XBee 2.4 GHz radio module. Power is supplied by a 70Watt solar panel and 35 Amp-Hour battery that allows nodes to run for at least one week of full overcast and completely recharge in one day of full sun. The complete hardware of a perimeter node installed at METEC is shown in Figure 2.

Figure 2: Perimeter Node Hardware

The gateway node utilizes a Beaglebone Black as the central processor an XBee 2.4 GHz radio module for communication with perimeter nodes. The gateway node was wired hard-wired to power and internet at METEC, but it could easily be connected to solar power and a cellular modem for deployment in remote locations. The reference node uses a similar setup to the gateway node, only replacing the XBee radio with a 16-bit ADC connected to a factory calibrated pyranometer.

The photodetector pyranometers fitted to all perimeter and reference nodes were built from kits purchased from the Institute for Earth Science Research and Education (David Brooks, 2007). Each photodetector pyranometer measures irradiance using a 470 Ω resistor soldered across the terminals of a PDB-C139 photodetector. The photodetector is fitted inside a PVC tube covered with a Teflon disk to evenly diffuse light from a wide range of solar zenith angles. The reference node is fitted with a factory calibrated Kipp & Zonen SP Lite 2 pyranometer that was taken as GHI truth. Comparing the photodetector to the reference pyranometer demonstrated a very strong linear correlation. Irradiance readings from the photodetector and reference pyranometers were measured simultaneously at 10 Hz for 72 consecutive hours. Comparing the two sets of readings yielded a correlation coefficient, $\rho=0.9993$, and a coefficient of determination, $R^2=0.9985$, as seen in Figure 3.

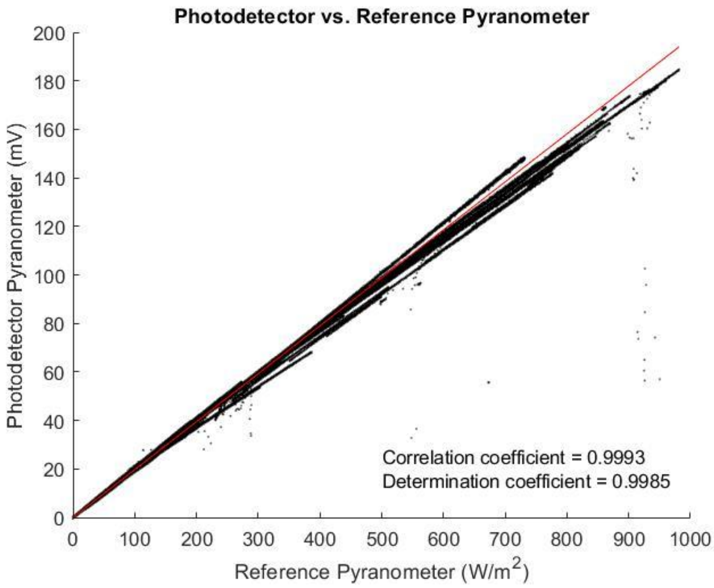

Figure 3: Photodetector Accuracy

3. Methods

This project compares two different CMV calculation methods. The first method used is the Most Correlated Pair (MCP) method as derived by Bosch et al. (Bosch et al., 2013). This method assumes that readings from two sensors are well correlated but yield the highest correlation coefficient when lagged by some non-zero amount in time. After calculating the time lag of maximum correlation for each pair of nodes, the pair of nodes with the highest correlation coefficient is assumed to be the most aligned with CMV direction. The azimuth between this most correlated pair of nodes is taken as the cloud direction azimuth and the speed is calculated by dividing the distance between the two nodes by the calculated time lag. Because this method has been well established, it is used as a benchmark comparison for the Simplex Cross-correlation Method (SCM).

SCM builds on the MCP method by making three assumptions about cloud shape and applying a simplex algorithm to further refine the CMV approximation. SCM uses the same three assumptions as the LCE method derived by Bosch et al. (Bosch et al., 2013), but applied to the entire array of pyranometers. It is assumed:

(i) Linear cloud edge across the sensor array
(ii) Constant CMV while passing over the sensor array
(iii) Cloud shadow passes over all sensors

For time periods less than 1 hour, (ii) generally holds true. For slow GHI transitions caused by passing stratus clouds (i) and (iii) almost always hold true with sensor spacing **O(**1 mile**)**. For sharp GHI transitions caused by passing cumulus clouds (i) and (iii) usually hold true for all sensors if maximum inter-sensor spacing **O(**100m**),** and a subset of sensors located along the cloud's path for larger spacings.

3.1 Irradiance as a Function of Cloud Motion Vector

The CMV is modeled as a traveling planar edge with a direction azimuth α, edge azimuth β, and speed v. Taking any arbitrary pair of nodes N_i and N_j, line d_{ij} is drawn from N_i to N_j. Angle ϴ is the azimuth angle of line d_{ij}. Given that a cloud edge crosses node N_i at time $t_i$and node N_j at time t_j, the time delta between the cloud edge crossing the two nodes Δt_{ij} is:

$$\Delta t_{ij} = t_j - t_i \qquad \text{(eq. 1)}$$

This time delta can be calculated by tracing the point on the cloud edge C_i that passes directly over node N_i to its position when the cloud edge crosses node N_j. This creates line d'_{ij} that represents the true distance the cloud travels in time Δt_{ij} as shown in Figure 4 so that:

$$d'_{ij} = \Delta t_{ij} * v \qquad \text{(eq. 2)}$$

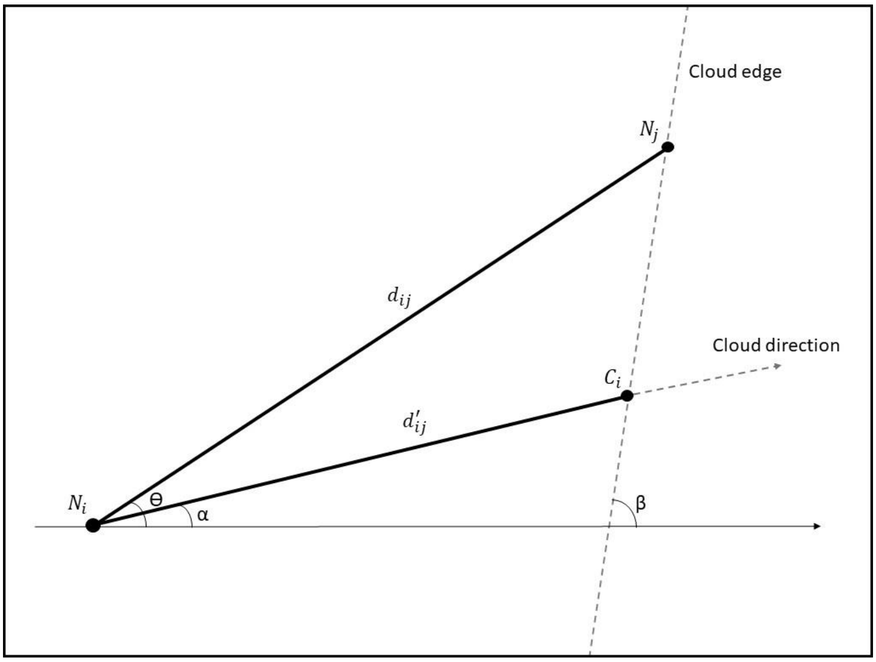

Figure 4: Cloud Crossing Geometry

The length of d'_{ij} can then be solved geometrically using a pair of right triangles such that:

$$d'_{ij} = d_{ij}\left[cos\left(\theta_{ij} - \alpha\right) - sin\left(\theta_{ij} - \alpha\right)\cot(\beta - \alpha)\right] \quad \text{(eq. 3)}$$

In the case that CMV direction is parallel to the cloud edge (eq. 3) is undefined but assuming (iii) this case is impossible as the cloud edge doesn't cross any nodes. In case that CMV direction is perpendicular to the cloud edge, equation (3) can be simplified to:

$$d'_{ij} = d_{ij}cos(\theta - \alpha) \quad \text{(eq. 4)}$$

Combining (eq. 2) and (eq. 3) gives the analytical solution for the time delta Δt_{ij} between the cloud edge crossing nodes N_i and N_j:

$$\Delta t_{ij} = \frac{d_{ij}[cos(\theta_{ij}-\alpha)-sin(\theta_{ij}-\alpha)\cot(\beta-\alpha)]}{v} \quad \text{(eq. 5)}$$

3.2 Cloud Motion Vector as a Function of Irradiance

A CMV is calculated from irradiance by comparing the matrix of measured time deltas $\boldsymbol{\Delta t}$ and the matrix of time deltas from an approximated CMV $\boldsymbol{\Delta t'}$ between every arbitrary pair of nodes. For each pair of nodes N_i and N_j an error measure of the CMV approximation e_{ij} is calculated as the squared difference between the measured and approximated time delta such that:

$$e_{ij} = \left\|\Delta t_{ij} - \Delta t'_{ij}\right\|^2 \quad \text{(eq. 6)}$$

Taking the sum of the matrix of individual error measures yields a total error measure for the CMV approximation:

$$E = \sum_{i,j}\left\|\Delta t_{ij} - \Delta t'_{ij}\right\|^2 \quad \text{(eq. 7)}$$

This total error measure can be expanded with (5) to create a CMV error function of variables α, β, and v:

$$E(\alpha, \beta, v) = \sum_{i,j}\left\|\Delta t_{ij} - \frac{d_{ij}[cos(\theta_{ij}-\alpha)-sin(\theta_{ij}-\alpha)\cot(\beta-\alpha)]}{v}\right\|^2 \quad \text{(eq. 8)}$$

Backing out the CMV from this error function is now a tri-variate minimization problem. An initial CMV guess is found using the pair of nodes most aligned with the cloud direction. The pair of nodes with the largest time delta containing the first and last nodes the cloud shadow crossed is assumed to be most aligned with CMV direction. Taking the first node crossed as N_i and the last node crossed as N_j, the initial guess cloud motion azimuth α_0 becomes the azimuth angle between the pair of nodes θ_{ij}. Cloud edge azimuth is predominantly orthogonal to the motion azimuth (Bosch et al., 2013), so β_0 is assumed to be perpendicular to α_0. The initial guess speed v_0 is then found by dividing the distance between nodes d_{ij} by the measured time lag Δt_{ij}. With this initial guess CMV, the error function (8) is minimized using the Nelder-Mead downhill simplex algorithm (Nelder and Mead, 1965). Other algorithms were considered, but the unstable Jacobian and Hessian of the error function rules out any gradient or quadratic algorithms.

3.3 Quality Control

Each individual sensor is not synchronized to measure GHI simultaneously, so the data from all sensors is first resampled to exactly 10 Hz. The resampled time series values are found using linear interpolation. To remove daily trend information caused by the solar position, measured irradiance is divided by the local clear-sky index generated using the PVLIB toolbox from Sandia National Laboratories (Stein et al., 2016).

Before attempting to calculate CMVs across a given window, it must first be determined if any detectable cloud edges occurred in that time window. The measured irradiance is first down-sampled to a 10 second interval to ignore small changes between readings. The Manhattan distance for this window is found by summing the discrete derivative of this down-sampled irradiance sequence. If the Manhattan distance is greater than the average clear sky index across the window it can be assumed that at least one sharp transition has taken place. To ensure (iii) holds true, CMVs are only calculated when all nodes see at least one sharp transition. This can be seen in Figure 5 where CMVS are not calculated during overcast periods, periods with full sun, and when a shadow passes over only one node.

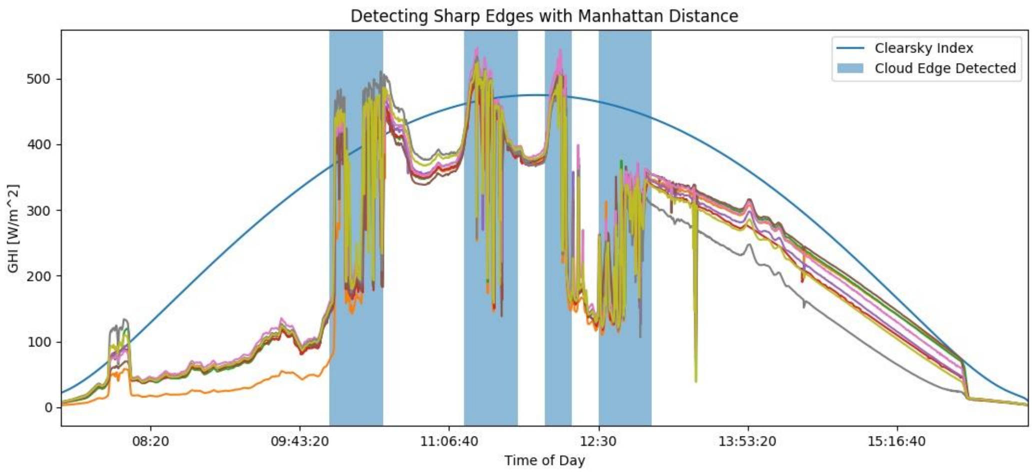

Figure 5: Manhattan Distance Example

Time deltas between nodes are calculated by maximizing the cross-correlation function between two sensors as defined by Bosch et al. (Bosch et al., 2013). The cross-correlation coefficient ρ_{ij} between the time series for two sensors is calculated at a range of time lags to create a function $\rho_{ij}(\Delta t)$. The time lag with the highest cross-correlation coefficient is taken as the time delta between the two nodes. To ensure (i) and (iii) hold true, poorly correlated sensor pairs must be removed. If the maximum cross-correlation coefficient for a pair of sensors $\rho_{ij} < 0.79$ the time delta between this pair is ignored when calculating CMVs.

3.4 Validation

Both methods were compared against validation data obtained by combining 449 MHz wind profiler observations from the NWS station located 51 kilometers Southeast in Platteville, CO (US Department of Commerce, n.d.) with ceilometer observations from the NOAA Automated Weather Observation Station (AWOS) located 20 kilometers Southeast at the Fort Collins-Loveland Regional Airport (National Centers for Environmental Information, n.d.). Combining observed cloud ceiling height with the wind profile speed and direction gives a reasonable estimate of CMVs passing over the test site. Because often multiple ceilings are reported with different heights and velocities, only times with one reported cloud ceiling are used for validation. The location of the AWOS ceilometer and Platteville wind profiler in comparison to METEC can be seen in Figure 6.

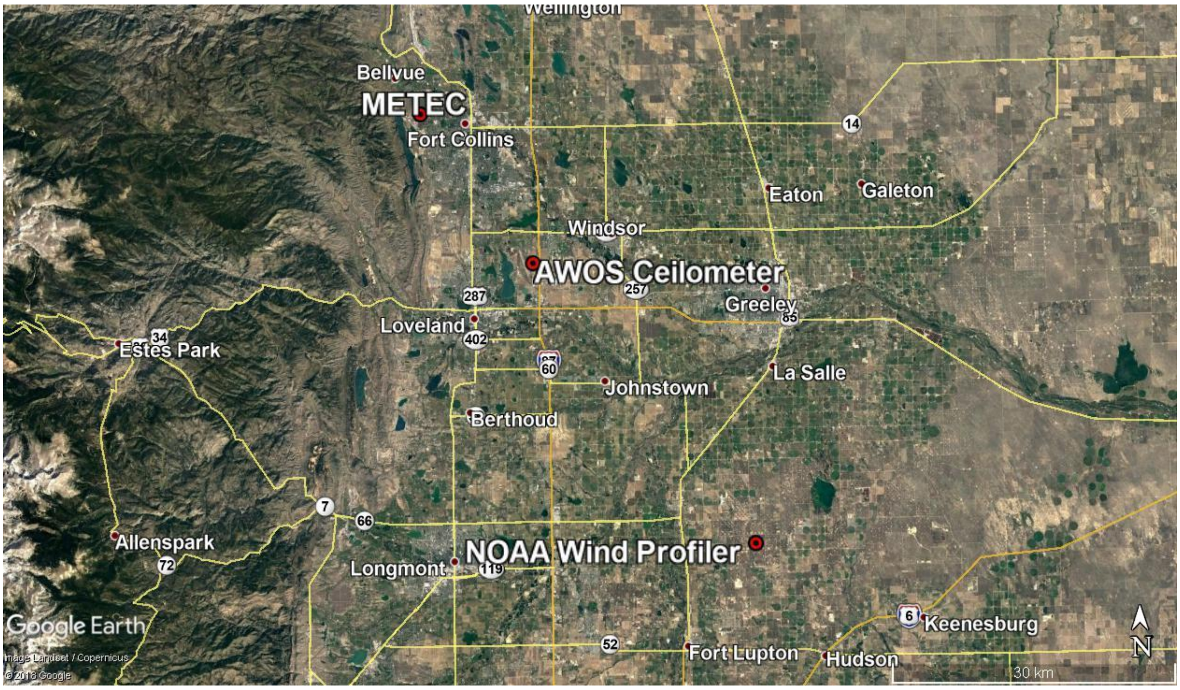

Figure 6: Validation Data Source Location

4. Results

CMVs were calculated across a rolling 15-minute window with a 5-minute step and any CMVs with velocity greater than 50 m/s are thrown out. The averaged CMVs were compared to validation data based on three metrics: Root-Mean Square Error (RMSE) (eq. 9), Mean Bias Error (MBE) (eq. 10), and the Pearson correlation coefficient of cloud speed and azimuth. Because cloud azimuth has no stable expected value over an extended period of time, MBE was only calculated for cloud speed.

$$RMSE = \sqrt{\frac{\sum_N (x_n - \bar{x}_n)^2}{N}} \qquad \text{(eq. 9)}$$

$$MBE = \frac{\sum_N (x_n - \bar{x}_n)}{N} \qquad \text{(eq. 10)}$$

Validation data was acquired for 10 months between September 2017 and June 2018. From this period, intermittent clouds were detected concurrently with reported validation data on 41 days yielding over 1200 CMV comparisons. Both CMV calculation methods performed comparatively well to validation data as shown in Figure 7. The calculated CMVs show a strong correlation with validation data in speed and azimuth.

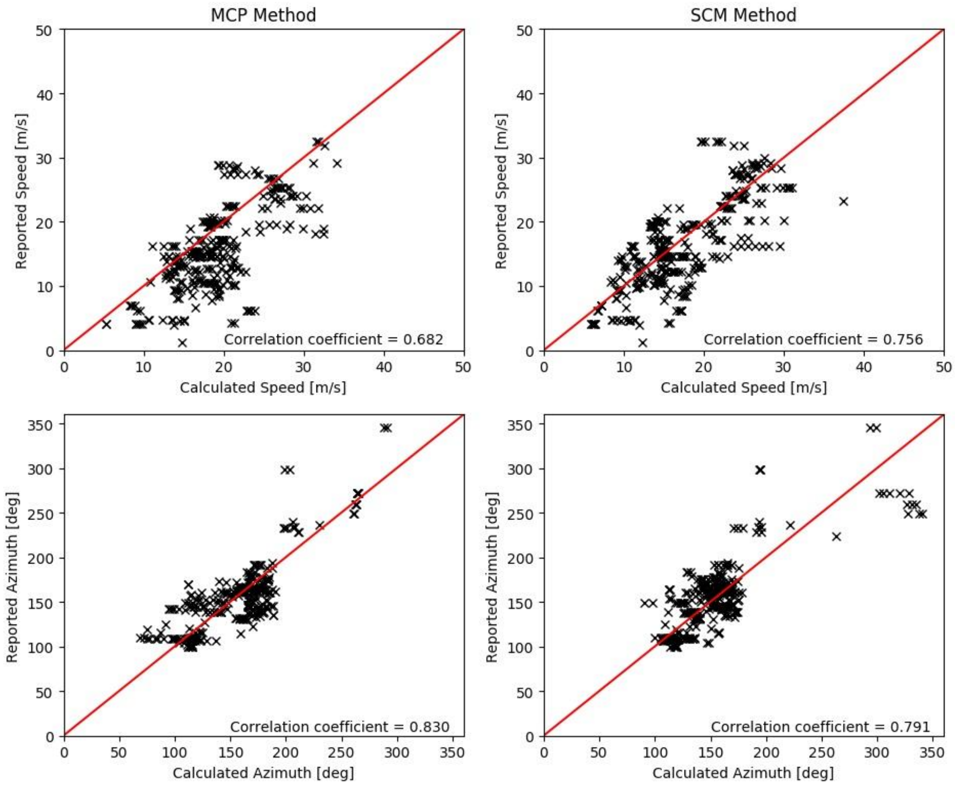

Figure 7: Calculated CMVs vs. Validation Data

The performance metrics of calculated CMVs against validation data is shown in Table 1. Both methods performed comparably in speed and azimuth RMSE, but the MCP method showed greater bias towards high speed measurements.

Table 1: Calculated CMV Performance vs. Validation Data

	MCP	SCM
Speed RMSE	4.54 m/s	3.54 m/s
Speed MBE	1.86 m/s	1.17 m/s
Speed Correlation Coefficient	0.682	0.756
Azimuth RMSE	17.7°	18.5°
Azimuth Correlation Coefficient	0.830	0.791

5. Conclusions

An IoT network of low-cost pyranometers was implemented at CSU's METEC facility consisting of 12 uncalibrated photodiode pyranometers and one factory calibrated pyranometer. after comparing CMVs calculated using the SCM and MCP method it was found that the network could approximate CMVs with a RMSE of around 5 m/s and 24° compared to validation data acquired from a fusion of ceilometer and profiler data. This type of network shows great promise in predicting irradiance for use in hybrid solar-diesel power systems.

While 12 nodes with photodetector pyranometers were installed at METEC, reliability issues in the XBee radio modules used resulted in data from a maximum of seven nodes to be used in calculating any CMV. In future iterations of this project, a more reliable radio module will be used to increase network efficiency and ensure that all nodes provide a reliable data stream for calculating CMVs. The newly developed SCM shows promise in improving calculated CMV accuracy over existing methods but requires some adjustment to provide consistent, measurable improvement. Techniques of approximating CMVs for non-linear cloud edges and multiple cloud layers with different velocities may also be explored.

6. References

Aryaputera, A.W., Yang, D., Zhao, L., Walsh, W.M., 2015. Very short-term irradiance forecasting at unobserved locations using spatio-temporal kriging. Sol. Energy 122, 1266–1278. https://doi.org/10.1016/j.solener.2015.10.023

Bosch, J.L., Zheng, Y., Kleissl, J., 2013. Deriving cloud velocity from an array of solar radiation measurements. Sol. Energy 87, 196–203. https://doi.org/10.1016/j.solener.2012.10.020

Brooks, D., 2007. Measuring Sunlight at Earth's Surface: Build Your Own Pyranometer [WWW Document]. Inst. Earth Sci. Res. Educ. URL http://www.instesre.org/construction/pyranometer/pyranometer.htm (accessed 6.12.18).

Chow, C.W., Urquhart, B., Lave, M., Dominguez, A., Kleissl, J., Shields, J., Washom, B., 2011. Intra-hour forecasting with a total sky imager at the UC San Diego solar energy testbed. Sol. Energy 85, 2881–2893. https://doi.org/10.1016/j.solener.2011.08.025

Chow, C.W., Belongie, S., Kleissl, J., 2015. Cloud motion and stability estimation for intra-hour solar forecasting. Sol. Energy 115, 645–655. https://doi.org/10.1016/j.solener.2015.03.030

Menzel, W.P., 2001. Cloud tracking with satellite imagery: From the pioneering work of Ted Fujita to the present. Bull. Am. Meteorol. Soc. 82, 33–47.

National Centers for Environmental Information, n.d. Automated Weather Observing System (AWOS) [WWW Document]. URL https://www.ncdc.noaa.gov/data-access/land-based-station-data/land-based-datasets/automated-weather-observing-system-awos (accessed 6.12.18).

Nelder, J.A., Mead, R., 1965. A Simplex Method for Function Minimization. Comput. J. 7, 308–313. https://doi.org/10.1093/comjnl/7.4.308

Stein, J.S., Holmgren, W.F., Forbess, J., Hansen, C.W., 2016. PVLIB: Open source photovoltaic performance modeling functions for Matlab and Python. IEEE, pp. 3425–3430. https://doi.org/10.1109/PVSC.2016.7750303

Suri, M., Cebecauer, T., Skoczek, A., Marais, R., Mushwana, C., Reinecke, J., Meyer, R., 2014. Cloud cover impact on photovoltaic power production in South Africa. Proc. SASEC.

Urquhart, B., Kurtz, B., Dahlin, E., Ghonima, M., Shields, J.E., Kleissl, J., 2015. Development of a sky imaging system for short-term solar power forecasting. Atmospheric Meas. Tech. 8, 875–890. https://doi.org/10.5194/amt-8-875-2015

US Department of Commerce, N., n.d. PSD Wind Profiler Data [WWW Document]. URL https://www.esrl.noaa.gov/psd/data/obs/sites/view_site_details.php?siteID=pvl (accessed 6.12.18).

Yang, D., Dong, Z., Reindl, T., Jirutitijaroen, P., Walsh, W.M., 2014. Solar irradiance forecasting using spatio-temporal empirical kriging and vector autoregressive models with parameter shrinkage. Sol. Energy 103, 550–562. https://doi.org/10.1016/j.solener.2014.01.024